CHEMISTRY OF MATERIALS
Article

Chem. Mater. **2009,** *21,* 4527–4540 4527
DOI:10.1021/cm901447z

Bending and Shell Formation of Tellurium Nanowires Induced by Thiols

T. S. Sreeprasad, A. K. Samal, and T. Pradeep*

DST Unit on Nanoscience, Department of Chemistry and Sophisticated Analytical Instrument Facility, Indian Institute of Technology Madras, Chennai 600 036, India

Received May 27, 2009. Revised Manuscript Received August 6, 2009

The reactivity of tellurium nanowires (Te NWs) with thiol-containing molecules was probed. Depending upon the presence or absence of the stabilizing surfactant in the solution, the product differs drastically. When excess surfactant was present, the reaction resulted in a core-shell-like structure. Through various spectroscopic and microscopic techniques, it was understood that there is a redox reaction between TeO_2, present on the NW surface, and thiols added into the solution that resulted in the reduction of TeO_2 to Te(0) with simultaneous oxidation of thiols to disulfides. Energy-dispersive analysis of X-rays (EDAX) confirmed that the shell has large sulfur and oxygen content. Raman spectra as well as the spectral image showed that the shell contains sulfur in the form of disulfides. Time-dependent Raman measurements established the redox nature of the conversion. The redox reaction was confirmed by X-ray photoelectron spectroscopy (XPS) also. When the excess surfactant was removed by repeated centrifugation, the addition of thiols resulted in the bending of NWs. The monodispersity as well as single crystallinity of the sample were affected. The bent NWs possessed many defects along the length as a consequence of the reaction. When excess surfactant was present in the solution, a combination of sodium dodecyl sulfate (SDS) and the formed disulfide were capable of capping the structures suitably, avoiding defects. But when excess surfactant is removed, the remaining SDS and disulfide were not enough to protect the surface well, creating more defect sites that resulted in the bending of the NWs. It appears that the enthalpy of the redox reaction at the surface contributes to the bending of the nanostructures.

Introduction

Miniaturization of electronics shrinks the components smaller and smaller. Nanomaterials are predicted to be the ideal candidates toward this drive. Nanoscale metals and semiconductors are fascinating because their properties can be tailored by changing the size, shape, dielectric constant of the medium, etc.[1] The photophysical properties of gold nanoparticles are excellent examples to illustrate this tailorability. Gold, golden yellow in its bulk, changes its color radically when the size reduces below 100 nm. Spherical nanoparticles of gold in the 20 nm size range appear wine red in aqueous solutions,[2] whereas at 2−3 nm diameter, they are brown.[3] This color change is due to the variation of surface plasmon resonance with size.[4] Another pronounced change in the case of gold is its change from metallic to semiconducting behavior when the size goes to subnanometer range. Such nanoparticles are usually referred to as "quantum clusters", which are semiconducting and are highly fluorescent because of molecular transitions.[5]

Because of the large surface to volume ratio, the reactivity of nanoparticles is largely enhanced compared to its bulk. In the nanoregime itself, reactivity depends on the shape of the nanoparticle. The introduction of anisotropic nanoparticles made it possible to investigate the shape dependent reactivity of nanoparticles. Reactivity can be directly correlated to the surface structure of the nanoparticles. Again, if we take gold as an example, spherical gold nanoparticles are largely made of the most stable {111}/{100} low index planes.[6] Because of the inherent isotropy, both in shape and surface structure, spherical nanoparticle shows an isotropic reactivity, i.e., the reaction happens in similar way in all directions.[7]

Anisotropic nanoparticles are interesting because of their size and shape-dependent optical properties, which

*Corresponding author. E-mail: pradeep@iitm.ac.in. Fax: 91-44-2257-0545/ 0509.

(1) (a) Henglein, A. *Chem. Rev.* **1989**, *89*, 1861. (b) Kamat, P. V. *J. Phys. Chem. B* **2002**, *106*, 7729.
(2) (a) Turkevich, J.; Stevenson, P. C.; Hillier, J. *Discuss. Faraday Soc.* **1951**, *11*, 55. (b) Enüstün, B. V.; Turkevich, J. *J. Am. Chem. Soc.* **1963**, *85*, 3317.
(3) Yao, H.; Minami, T.; Hori, A; Koma, M.; Kimura, K. *J. Phys. Chem. B* **2006**, *110*, 14040.
(4) Schasfoort, R. B. M.; Tudos, A. J. *Handbook of Surface Plasmon Resonance*; RSC Publishing: London, 2008.
(5) (a) Ingram, R. S.; Hostetler, M. J.; Murray, R. W.; Schaaff, T. G.; Khoury, J. T.; Whetten, R. L.; Bigioni, T. P.; Guthrie, D. K.; First, P. N. *J. Am. Chem. Soc.* **1997**, *119*, 9279. (b) Schaaff, T. G.; Whetten, R. L. *J. Phys. Chem. B* **2000**, *104*, 2630. (c) Shibu, E. S.; Muhammed, M. A. H.; Tsukuda, T.; Pradeep, T. *J. Phys. Chem. C* **2008**, *112*, 12168. (d) Muhammed, M. A. H.; Shaw, A. K.; Pal, S. K.; Pradeep, T. *J. Phys. Chem. C* **2008**, *112*, 14324. (e) Shichibu, Y.; Negishi, Y.; Tsunoyama, H.; Kanehara, M.; Teranishi, T.; Tsukuda, T. *Small* **2007**, *3*, 835. (f) Muhammed, M. A. H.; Ramesh, S.; Sinha, S. S.; Pal, S. K.; Pradeep, T. *Nano Res.* **2008**, *1*, 333.
(6) Wang, Z. L. *J. Phys. Chem. B* **2000**, *104*, 1153.
(7) Tom, R. T.; Pradeep, T. *Langmuir* **2005**, *21*, 11896.

Published on Web 08/28/2009

find a plethora of applications in diverse fields.[8] Various anisotropic nanoparticles such as rods,[9] discs,[10] plates,[11] triangles,[12] wires,[13] flowers,[14] etc., have been reported. Most of the synthetic methods follow a template-mediated growth. For example, gold nanorods (GNRs) are made with the aid of a tubular micelle made up of cetyltrimethylammonium bromide (CTAB), which acts as a template for the growth of GNRs.[15] Recently, our group reported the synthesis of various anisotropic particles using polyaniline as a template.[11a] In all these processes, the directional growth is also aided by the absorption of surfactant to specific planes making the growth occur in other directions.[16] In the case of gold nanorods, because CTAB has a higher affinity toward the {110} plane, it attaches more to this plane and growth happens anisotropically and in the GNRs formed, the side faces are composed of {110} and the tips by either {111} or {100}.[17] So by the attachment of CTAB on to {110}, it gets extra stability and so this facet becomes prominent in GNRs even though it is energetically unstable.[17] The higher energy {110} is more prone to reaction. We probed this reactivity difference on GNR surface.[18] Upon addition of Cu^{2+} into the GNR solution, depending upon the presence or absence of excess surfactant, the reaction differs.[18] We found that the presence of extra stabilizing agent makes the reaction start from the rod tip; after centrifugation to remove excess surfactant, the reaction starts from the rod body.[18]

One-dimensional (1D) nanostructures like nanowires, nanorods, nanobelt, and nanotubes are attractive because they find direct application in the field of electronics.[19] Nanowires are said to be the perfect contenders for studying the dependence of optical, electrical, magnetic, and mechanical properties on size confinement.[13] One of the key features of nanowire (NW) morphology is that properties like electron conduction are allowed only in one direction and confined in all others. The inherent confinement of conduction along the short axis makes them interesting candidates for ballistic electron transfer.[20] A wide variety of materials such as metals and semiconductors have been used to make NWs.[21] Among the various semiconducting materials, trigonal-tellurium (t-Te), which is a p-type semiconductor and has a very narrow band gap, has attracted a great deal of interest because of its good photoconductivity, photoelectricity, thermoelectricity, catalysis, nonlinear optical properties, and high piezoelectricity. These make it a viable candidate for many important applications.[22] The reduction potential of TeO_3^{2-}/Te system is around 0.589 V.[23] Hence, recently Te nanowires (Te NWs) were considered as templates for making metal composites with metals having favorable reduction potentials with respect to this couple.[23]

Unlike GNR, synthesis of Te NW is comparatively simpler. Due to the unique crystal structure which has a helical-chain conformation, Te has a very high tendency to grow anisotropically.[24] It has been believed that in a hexagonal lattice, Te atoms are bound together through van der Waals interactions to form 1D structures. Several methods such as thermal deposition,[25] hydrothermal,[26] microwave-assisted,[27] and biomolecule-assisted[28] syntheses and chemical vapor deposition[29] have been reported for the synthesis of Te NWs. Most of them were done at very high temperatures. Recently, Lin et al. reported a room-temperature, high-yield synthesis of Te NWs, where because of the inherent anisotropic crystal structure, NWs are getting formed in solution upon reduction with hydrazine without the aid of any template.[24] The

(8) (a) El-Sayed, M. A. *Acc. Chem. Res.* **2001**, *34*, 257. (b) El-Sayed, M. A. *Acc. Chem. Res.* **2004**, *37*, 326. (c) Jain, P. K.; Eustis, S.; El-Sayed, M. A. *J. Phys. Chem. B* **2006**, *110*, 18243. (d) Jain, P. K.; Huang, X.; El-Sayed, I. H.; El-Sayed, M. A. *Acc. Chem. Res.* **2008**, *41*, 1578.

(9) (a) Yu, Y. Y.; Chang, S. S.; Lee, C. L.; Wang, C. R. C. *J. Phys. Chem. B* **1997**, *101*, 6661. (b) Van der Zande, B. M. I.; Bohmer, M. R.; Fokkink, L. G. J.; Schonenberger, C. *J. Phys. Chem. B* **1997**, *101*, 852. (c) Kim, F.; Song, J. H.; Yang, P. D. *J. Am. Chem. Soc.* **2002**, *124*, 14316. (d) Wang, C.; Chen, Y.; Wang, T.; Ma, Z.; Su, Z. *Chem. Mater.* **2007**, *19*, 5809.

(10) Hanarp, P.; Kall, M.; Sutherland, D. S *J. Phys. Chem. B* **2003**, *107*, 5768.

(11) (a) Sajanlal, P. R.; Sreeprasad, T. S.; Sreekumaran Nair, A.; Pradeep, T. *Langmuir* **2008**, *24*, 4607. (b) Porel, S.; Singh, S.; Radhakrishnan, T. P. *Chem. Commun.* **2005**, 2387.

(12) (a) Kim, F.; Connor, S.; Song, H.; Kuykendall, T.; Yang, P. *Angew. Chem., Int. Ed.* **2004**, *43*, 3673. (b) Millstone, J. E.; Park, S.; Shuford, K. L.; Qin, L.; Schatz, G. C.; Mirkin, C. A. *J. Am. Chem. Soc.* **2005**, *127*, 5312. (c) Sajanlal, P. R.; Pradeep, T. *Adv. Mater.* **2008**, *20*, 980.

(13) (a) Hu, J. T.; Odom, T. W.; Lieber, C. M. *Acc. Chem. Res.* **1999**, *32*, 435. (b) Wiley, B.; Sun, Y.; Mayers, B.; Xia, Y. *Chem.—Eur. J.* **2005**, *11*, 454. (c) Sun, Y.; Xia, Y. *Science* **2002**, *298*, 2176. (d) Goldberger, J.; Fan, R.; Yang, P. *Acc. Chem. Res.* **2006**, *39*, 239.

(14) Sajanlal, P. R.; Pradeep, T. *Nano Res.* **2009**, *2*, 306.

(15) Sau, T. K.; Murphy, C. J. *Langmuir* **2004**, *20*, 6414.

(16) (a) Juste, J. P.; Santos, I. P.; Liz-Marz′an, L. M.; Mulvaney, P. *Coord. Chem. Rev.* **2005**, *249*, 1870. (b) Gole, A.; Murphy, C. J. *Chem. Mater.* **2005**, *17*, 3668.

(17) (a) Wang, Z. L.; Gao, R. P.; Nikoobakht, B.; El-Sayed, M. A. *J. Phys. Chem. B* **2000**, *104*, 5417. (b) Hernandez, J.; Solla-Gullon, J.; Herrero, E.; Aldaz, A.; Feliu, J. M. *J. Phys. Chem. B* **2005**, *109*, 12651.

(18) Sreeprasad, T. S.; Samal, A. K.; Pradeep, T. *Langmuir* **2007**, *23*, 9463.

(19) Ferry, D. K. *Science* **2008**, *319*, 579.

(20) Zhou, X.; Dayeh, S. A.; Aplin, D.; Wang, D.; Yu, E. T. *Appl. Phys. Lett.* **2006**, *89*, 053113.

(21) Xia, Y.; Yang, P.; Sun, Y.; Wu, Y.; Mayer, B.; Gates, B.; Yin, Y.; Kim, F.; Yan, H. Q. *Adv. Mater.* **2003**, *15*, 353.

(22) (a) Xia, Y.; Yang, P.; Sun, Y.; Wu, Y.; Mayer, B.; Gates, B.; Yin, Y.; Kim, F.; Yan, H. Q. *Adv. Mater.* **2003**, *15*, 353. (b) Huang, M. H.; Mao, S.; Feick, H.; Yan, H.; Wu, Y.; Kind, H.; Weber, E.; Russo, R.; Yang, P. *Science* **2001**, *292*, 1897. (c) Duan, X.; Huang, Y.; Cui, Y.; Wang, J.; Lieber, C. M. *Nature* **2001**, *409*, 66.

(23) (a) Wang, Y.; Tang, Z.; Podsidlo, P.; Elkasabi, Y.; Lahann, J.; Kotov, N. A. *Adv. Mater.* **2006**, *18*, 518. (b) *Lange's Handbook of Chemistry*, 13th ed.; Dean, J. A, Ed.; McGraw-Hill: New York, 1985; Sect. 8. (c) Lin, Z.-H.; Chang, H.-T. *Langmuir* **2008**, *24*, 365. (d) Lin, Z.-H.; Lin, Y.-W.; Lee, K.-H.; Chang, H.-T *J. Mater. Chem.* **2008**, *18*, 2569. (e) Zhang, B.; Hou, W. Y.; Ye, X. C.; Fu, S. Q.; Xie, Y. *Adv. Funct. Mater.* **2007**, *17*, 486. (f) Jiang, X.; Mayers, B.; Herricks, T.; Xia, Y. *Adv. Mater.* **2003**, *15*, 1740.

(24) (a) Lin, Z.; Yang, Z.; Chang, H. *Cryst. Growth Des.* **2008**, *8*, 351. (b) Mayers, B.; Xia, Y. *J. Mater. Chem.* **2002**, *12*, 1875. (c) Mayers, B.; Xia, Y. *Adv. Mater.* **2002**, *14*, 279. (d) Gautam, U. K.; Rao, C. N. R. *J. Mater. Chem.* **2004**, *14*, 2530.

(25) Yu, H.; Gibbons, P. C.; Buhro, W. E. *J. Mater. Chem.* **2004**, *14*, 595.

(26) (a) Mo, M.; Zeng, J.; Liu, X.; Yu, W.; Zhang, S.; Qian, Y. *Adv. Mater.* **2002**, *14*, 1658. (b) Liu, Z.; Li, S.; Yang, Y.; Hu, Z.; Peng, S.; Liang, J.; Qian, Y. *New J. Chem.* **2003**, *27*, 1748. (c) Xi, G.; Peng, Y.; Yu, W.; Qian, Y. *Cryst. Growth Des.* **2005**, *5*, 325.

(27) Zhu, Y. J.; Wang, W. W.; Qi, R. J.; Hu, X. L. *Angew. Chem.* **2004**, *116*, 1434.

(28) (a) Lu, Q.; Gao, F.; Komarneni, S. *Adv. Mater.* **2004**, *16*, 1629. (b) He, Z.; Yu, H. S.; Zhu, J. *Chem. Mater.* **2005**, *17*, 2785.

(29) (a) Geng, B.; Lin, Y.; Peng, X.; Meng, G.; Zhang, L. *Nanotechnology* **2003**, *14*, 983. (b) Mohanty, P.; Kang, T.; Kim, B.; Park, J. *J. Phys. Chem. B* **2006**, *110*, 791.

surfactants were added in order to arrest the reaction and to stabilize the formed structures.[24]

Te NWs are known to react with metals having favorable reduction potentials and to form composites.[23] Recently, we probed the reactivity of Te NWs through their reaction with graphite oxide (GO).[30] We found that upon mixing specific quantities of GO and Te NW, GO gets converted into leaf-like graphenic structures and Te NWs gets oxidized to TeO_3^{2-}. Time-dependent TEM showed that Te NWs are getting etched away continuously. In the beginning, they formed bent NWs because of the reaction and after 36 h, reacted almost completely into TeO_3^{2-}. Here, unlike GNR, interestingly the rod body was reacting first. This is expected because in the case of GNRs, CTAB forms a thick double layer around the rod body, preventing it from getting affected by external agents. Also, the removal of CTAB from this side faces is reported to be quite difficult. But in the case of Te NW, the protecting agent, sodiumdodecyl sulfate (SDS), is merely covering the surface and protecting it from getting aggregated.[24] Therefore, when an external agent comes, it prefers the sides and SDS can be displaced.

Thiols are known to etch gold surfaces.[5] We have recently used the etching reaction between thiols and gold nanoparticles to form molecular clusters.[5f] Thiols are known to assemble GNRs also.[31] Recently we found that the addition of dimercaptosuccinic acid (DMSA) into GNRs in definite concentrations can give rise to different well-arranged superstructures.[31b] The electrostatic neutralization between DMSA and CTAB, which covers the GNRs, was found to make GNR assemble into different superstructures.[31b] Because the covering of GNR is thick, strong, and positive in electrical charge, this kind of an assembly was possible.

Reactivity of NWs is a poorly investigated area. Only reactions with metals have been explored. In the case of Te NW the reactivity with metals leading to the formation of tellurides has been investigated.[23] Reactivity with metalloids such as sulfur has not been probed. In this report, we examined the reactivity of Te NWs with different molecules containing thiol groups, taking DMSA as the model system. We found that the chemistry and the resultant product can be changed by controlling the concentration of surfactant present in the reaction mixture. We report a reaction between Te NW and DMSA which can either form a core-shell-like structure or bend the NWs, depending upon the concentration of the surfactant present in the system. When excess SDS was present in the reaction mixture, a core−shell structure was formed, whereas when the excess surfactant was removed by centrifugation and thiols are added, NWs were found to bend. The reaction was followed by UV/vis spectroscopy, Raman spectroscopy, X-ray photoelectron spectroscopy (XPS), transmission electron microscopy (TEM), and energy-dispersive analysis of X-rays (EDAX). A novel redox-like reaction between TeO_2 present on the NW surface and thiol is suggested to be the reason for the changes.

(30) Sreeprasad, T. S.; Samal, A. K.; Pradeep, T. *J. Phys. Chem. C* **2009**, *113*, 1727.
(31) (a) Gole, A.; Orendorff, C. J.; Murphy, C. J. *Langmuir* **2004**, *20*, 7117. (b) Sreeprasad, T. S.; Samal, A. K.; Pradeep, T. *Langmuir* **2008**, *24*, 4589.

Experimental Section

Materials. Sodium dodecyl sulfate (SDS, $C_{12}H_{25}O_4SNa$, 99%) was obtained from Acros. Tellurium dioxide powder (99.9%) was purchased from Alfa Aesar. Hydrazine monohydrate ($N_2H_4.H_2O$, 99−100%) and salicylic acid (SA) were purchased from SD Fine chemicals, India. Dimercaptosuccinic acid (DMSA), mercaptosuccinic acid (MSA), mercaptopropionic acid (MPA), propane thiol (PT), cysteine, butanol, and isopropyl amine (IPA) were purchased from Sigma-Aldrich. All chemical were used as received without any additional purification. Triply distilled water was used all through this study.

Methods. The UV/vis spectrum of each sample was measured by using a Perkin-Elmer Lambda 25 UV/vis spectrophotometer. For all TEM measurements, the reaction mixture was drop-casted onto a carbon-coated copper grid and dried in ambient conditions. These samples were examined with a JEM 3011 (JEOL Ltd.), 300 kV high-resolution transmission electron microscope (HRTEM) with a UHR polepiece. Raman spectra were measured with a WiTec GmbH confocal micro Raman spectrometer. XPS measurements were done with Omicrometer ESCAProbe spectrometer with unmonochromatized Al Kα X-rays ($h\nu$ = 1486.6 eV). Six spectra in the desired binding energy range were averaged. The samples were spotted as drop cast films on the sample stub and dried. X-ray flux was adjusted to reduce the beam-induced damage of the sample. The energy resolution of the spectrometer was set at 0.1 eV at a pass energy of 20 eV for typical measurements.

Synthesis of Te NW followed the reported method by Lin et al.[24] In short, TeO_2 powder was slowly reduced using hydrazine hydrate in a beaker under constant stirring. After 1 h, the color changed from colorless to blue, indicating the formation of Te NWs. SDS was added to this solution to arrest the reaction and to protect the Te NWs formed.

The experiments were done with two types of Te NW samples. The as-prepared dispersion was centrifuged at 8 000 rpm in a 40 mL centrifuging tube for 15 min to remove excess hydrazine and SDS. The once-centrifuged sample was redispersed in an equal amount of distilled water. This will be referred to as Te_1 and was treated with thiol-containing molecules. Another type of Te NW sample (referred to as Te_2) was also prepared. Here the as-prepared sample was put through four cycles of centrifugation and redispersion cycles and after the final round of centrifugation, the sample was made up to half of the initial volume. Different thiol molecules were then added to study the reactivity.

Results and Discussion

Figure 1A shows the UV/vis spectrum Te NW after removing the excess surfactant and impurities by one round of centrifugation and redispersion in distilled water (Te_1). Te NW is known to have two characteristic peaks in the UV/vis spectrum.[24] The transition from p-bonding valence band (VB_2) to the p-antibonding conduction band (CB_1) is known to show a characteristic feature around 280−300 nm, known generally as peak I. The second feature referred to as peak II is due to the transition from the p-lone

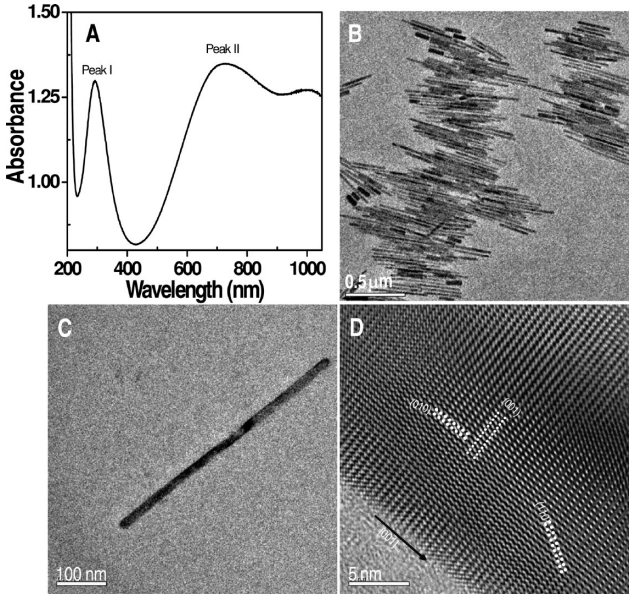

Figure 1. (A) UV/vis spectrum of pristine Te NWs after one time centrifugation and redispersion to initial volume in distilled water. (B) Large-area TEM micrograph of the pristine Te NWs showing a straight morphology, devoid of any shells. (C) High-magnification TEM image of a single Te NW devoid of any shell or bend. (D) Lattice-resolved image of the body of a single Te NW with lattice planes marked with dotted lines. We can see that the wire body is devoid of any defect and the sides are well-structured without any coating.

pair valence band (VB_3) to the p-antibonding conduction band (CB_1), which comes around 650−750 nm.[24a] As length of the NW increases, peak II will shift to a higher wavelength region. In a particular synthesis, peak I was centered at 293 nm and peak II was centered at 720 nm. Figure 1B shows the large-area TEM image of Te NWs after purification by centrifugation and redispersion to initial volume (Te_1). We can see that the wires are mostly monodisperse, straight and pretty clean devoid of any kind of coating. Length of the NWs was around 600 nm and the diameter was in the range of 15−25 nm. Figure 1C shows a HRTEM image of a single Te NW. We can see that the NW is straight and devoid of any covering. Figure 1D shows a lattice-resolved HRTEM image of one side of a Te NW. The three representative planes of t-Te NWs, with interplanar spacings of 0.59, 0.39, and 0.22 nm corresponding to {001}, {010}, and {110}, respectively, are marked in the figure by dotted lines.[24a] The crystals were structurally uniform and there were no defects, indicating that the t-Te NWs are single crystals. The sides were very clean without any debris or defects and even the sidewall atoms were clearly seen as a part of the continuing lattice from the rod body, emphasizing the single-crystalline nature of the sample.

Figure 2 shows the UV/vis spectral changes upon the addition of different thiols to the Te NW (Te_1) solution. Figure 2A shows the spectral changes accompanied by the addition of DMSA. Pristine NWs showed peak I at 293 nm and peak II at 720 nm. Calculated amounts of thiols were added into the NW solution to obtain the required final concentration of thiols indicated on the figures. After the addition of thiols, there was a blue shift in peak I position and a smearing of the peak also was observed. This was common for all thiol molecules tried. In the case of DMSA, in presence of 0.5 mM DMSA, peak I shifted to 284 nm. When 2 mM DMSA was present in the Te NW, peak I almost became a hump and the peak position was shifted to ~274 nm. After this, the addition of DMSA did not show any appreciable shift in the peak position. At a concentration of 5 mM of DMSA, peak I almost became a shoulder. Peak II was found to be unaffected by the addition DMSA.

Similar trends were observed for all thiol-containing molecules like MSA, MPA, and PT. In all the cases, as the concentration increased, peak I got flattened, whereas peak II remained unaffected. Because PT was not fully soluble in water, ethanol was used as the solvent. The changes seen around peak II in the case of PT are believed to be due to this change in solvent polarity. But overall, the changes seen were quite consistent with other observations. In the as-prepared Te NW samples before centrifugation, peak I is sometimes absent. This can be due to the presence of excess surfactant. After one centrifugation−redispersion cycle, we clearly see two distinct features in the UV/vis spectrum; upon the addition of thiols, as the concentration increased, peak I was getting flattened out. So the cause of this dampening can be the increase in the local concentration of surfactant because of the reaction with thiols leading to a probable coating around the NWs. Thiols can have a contribution to the UV/vis spectra in the lower wavelength region. The smearing on peak I may be an effect of the increased absorbance of thiols in this region. To verify this aspect, we compared the spectrum of pure DMSA (0.5 mM) to that of the spectrum of Te NW sample containing 0.5 mM DMSA (see the Supporting Information, Figure S2). It showed that in the case of Te NWs, the increase in intensity did not exactly coincide with that of the thiol spectrum. However, at very low wavelengths, below 225 nm, there was a one-to-one correspondence between the two spectra. This shows that the smearing of peak I is not entirely due to the absorption of thiols. Also, the parent Te NW sample before centrifugation had a smeared peak I. Peak I was observed only after centrifuging the sample to remove the excess surfactant. So the smearing of peak I in this case may be due to the increase in local concentration of the surfactant. At very high concentrations, thiols can have an effect on the spectra. But the difference in the spectra of Te NW sample containing thiol and that of pure thiol as well as the observation that the Te NW sample before centrifugation (which did not contain any thiol) showed a similar smearing of peak I point to the fact that the increase in the covering of Te NW locally because of the formed core−shell structure also contributes to the visible changes. It has to be noted that there was a shift in the position of peak I associated with the smearing of peak I. If the changes seen in the spectra were entirely due to thiol absorption, such a shift would not have been observed. In the case of gold nanorods, such a shift in the transverse surface plasmon band is known to be due to the increase in breadth and so a decrease in aspect ratio.[8c] In the

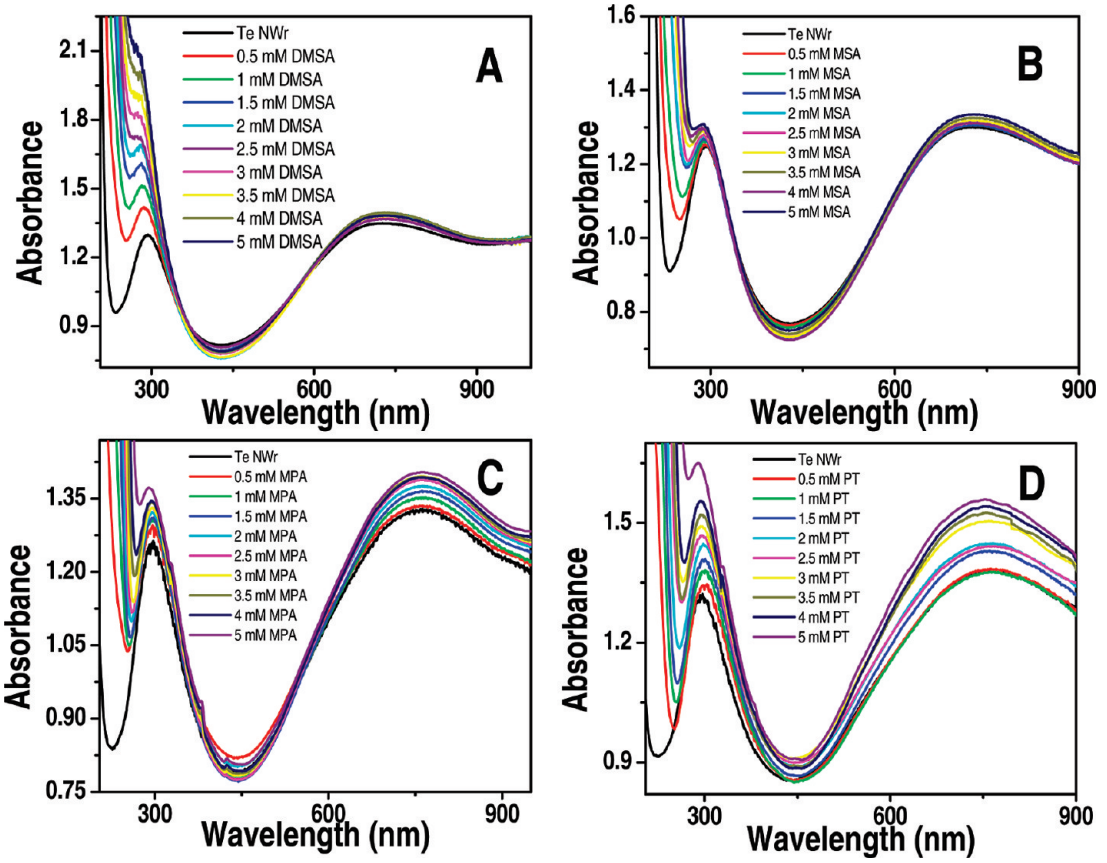

Figure 2. UV/vis spectral changes of Te NW as a function of concentration of (A) DMSA, (B) MSA, (C) MPA, and (D) PT. In the spectra, we can see that as the thiols are added into Te NW, peak I of the NW is getting ill-defined, which is more evident in A and B. At a concentration of 5 mM of thiol, peak I almost got fully flattened out.

present case, because of the formation of a thick shell, the core−shell structure has a higher effective diameter compared to that of parent Te NW. So the shift may also be attributed to the increase in effective diameter.

Different molecules having different functionalities were treated with the NW sample to examine whether the chemistry is unique to thiol containing molecules (see the Supporting Information, Figure S1). Nanowires were treated with a biomolecule, cysteine, which is an amino-acid containing a thiol group. It has amino and carboxylic acid groups in addition to thiol. It showed a similar trend as other thiol-containing molecules examined, emphasizing that the chemistry is possible in presence or various other functionalities also. Some molecules that do not contain thiol functionalities were also examined. Isopropyl amine (IPA), which contains only an amino group, did not show any characteristic change in the UV/vis spectrum. Peak I and II of Te NW remained almost unaffected after the addition of IPA. Similarly, salicylic acid (SA) and butanol, which have only a carboxylic acid and hydroxyl group, respectively, were treated with Te NW. Both these molecules did not show any reactivity with Te NW, proving that the chemistry is unique to the thiol group.

The samples were examined using HRTEM to find out the structural changes upon reaction with DMSA. Figure 3 shows the TEM images taken from the sample that had 2 mM DMSA. Figure 3A shows a large-area TEM

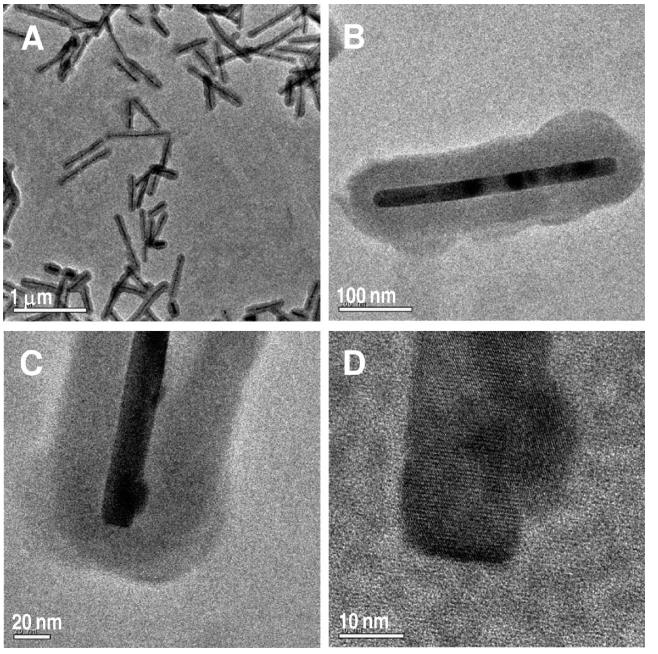

Figure 3. TEM images of "core−shell-like" structures formed in presence of 2 mM DMSA. (A) Large area image, (B) a single NW with core−shell structure, (C) expanded view of the tip of a single NW, and (D) lattice resolved image of the tip of a single NW.

image of the sample. We can see that all the Te NWs, which were clean in the parent solution (Figure 1), have acquired a "core−shell-like" structure upon reaction. The

sample was mostly monodisperse even after the reaction with uniform shell thickness. Figure 3B shows a single Te NW in greater detail. We can see a well-defined shell around it. The NW had a diameter of 15 nm and the shell thickness was around 30 nm. The shell was found to be uniformly distributed around the Te NW in all directions. Figure 3C shows the tip of a Te NW where an overgrowth can be seen. In Figure 3D the lattice-resolved image of the same portion is shown. Because of the presence of a thick shell, high-quality imaging was difficult. However, we obtained a reasonable image. Projections seen on the nanowires also showed the Te lattice, confirming that they are also due to Te. The most probable process occurring at the surface is the reduction of tellurium oxide present on the Te NW surface.[30] When the local concentration of tellurium oxide is larger, a protrusion occurs. Shell formation was a common observation for all the thiols examined. UV/vis changes, the smearing of peak I and the shift in its position, were seen immediately after the addition of thiols into the Te NW solution. So the reaction should be a fast process. All redox processes are expected to be fast. TEM imaging of the samples in a time-dependent fashion did not reveal any useful information. All the analyzed samples showed well-developed shells. The solvent being water, the time taken for complete drying of the sample was at least 12 h. Shorter drying times made the samples incompatible for vacuum. So all samples that were at least 12 h old thus showed a well-defined shell. The time dependence of the shell formation was not evaluated, but the extent of shell depends upon the specific thiol used. The shell was well-defined and most prominent in the case of DMSA. As a result, that system was examined in detail.

The effect of DMSA concentration on the shell formation was studied in detail using HRTEM. We added different amounts of DMSA into Te NW, and the sample was analyzed using HRTEM. Figure 4A shows a large-area image of Te NW without the addition of DMSA (zero concentration). We can see that the NWs are devoid of any covering and are clean. This is again emphasized in the higher-magnification image shown in Figure 4B. Figure 4C is a representative large-area image of sample containing 0.5 mM DMSA. We can see that the shells are beginning to form. Figure 4D shows the higher-magnification image of the same sample. In the figure, we can see a clear shell around the Te NWs. As the concentration of DMSA was increased, we found that the shell thickness is also increased. Figure 4E shows a large-area image of the Te NW sample which contains 2 mM DMSA. We can see that the shell thickness has increased more than that containing 0.5 mM DMSA. Figure 4F shows this aspect in greater detail. A comparison of images B, D, and F clearly establishes that the shell thickness increases as the concentration of DMSA increases. A similar trend was observed in all thiol molecules investigated. At 5 mM DMSA, a thick layer was seen all over the TEM grid and no clear image was obtained.

The mechanism of shell formation is still not fully clear. We did not see any shell when the surfactant was removed by repeated centrifugation. Because the shell was seen only with excess surfactant, we believe that the formed shell may be a combination of both DMSA and SDS. To know the elemental composition of the shell, we examined the sample (2 mM DMSA) with EDAX.

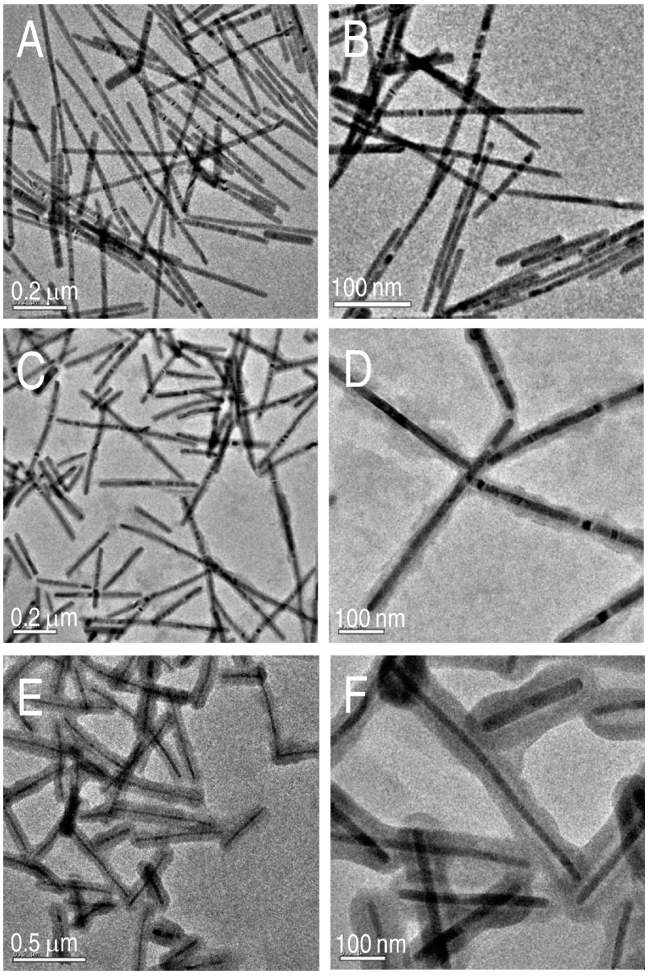

Figure 4. TEM images showing the effect of DMSA concentration on shell thickness (A, B) 0 mM DMSA, (C, D) 0.5 mM DMSA, and (E, F) 2 mM DMSA.

Figure 5 shows the EDAX spectrum and the corresponding elemental maps of core−shell-like structures. The EDAX spectrum clearly showed a high level of sulfur in the sample. The intensity of sulfur peak in the spectrum was larger compared to the Te peak itself. This points to the higher extent of sulfur in the sample compared to Te_1, which showed lower intensity (see the Supporting Information, Figure S3). The presence of tellurium, oxygen and carbon also can be seen in the spectrum. An elemental map of the sample also was done. It showed that the shell is mainly made of sulfur and oxygen. We can clearly see in the TEM micrograph that the thickness of the shell is greater compared to the diameter of the Te NW. It was seen in the elemental maps too. The Te map showed a similar thickness to that of the parent Te NW sample. Sulfur and oxygen maps showed higher thickness compared to the Te map indicating that the shell is made up of sulfur and oxygen and is devoid of Te. The surfactant used in Te NW synthesis, SDS, as well as the thiol added,

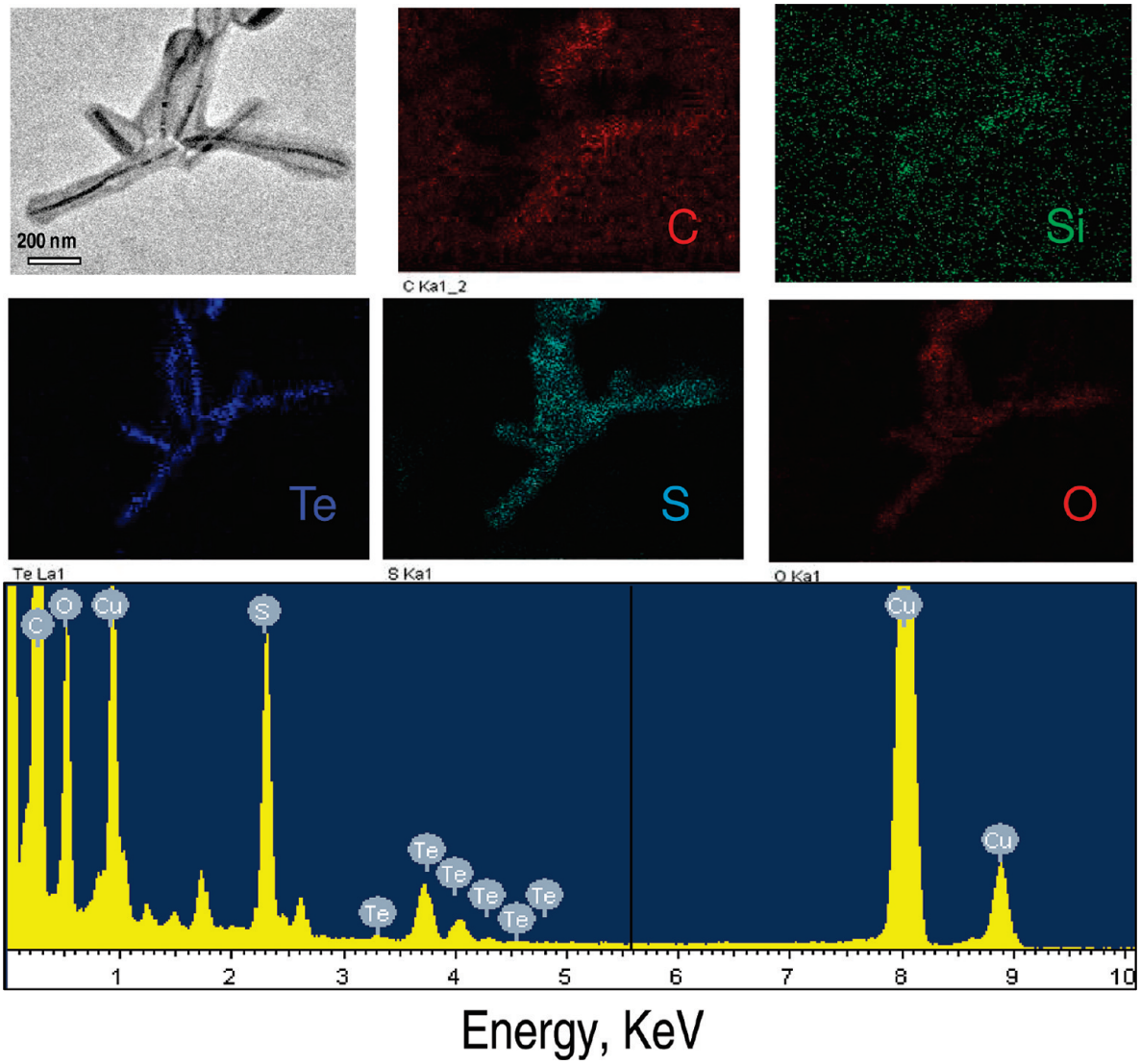

Figure 5. EDAX spectrum and elemental maps of the sample containing 2 mM DMSA showing the presence of a shell, which is mainly composed of sulfur and oxygen. The carbon content in the EDAX spectrum is larger in view of the carbon grid used. Cu is also due to the grid.

DMSA, has oxygen and sulfur in them. Hence, it is not sure whether the sulfur and oxygen shown in the spectrum are from the surfactant or from DMSA. But the most probable case is that a combination of both is responsible for the higher intensity shown in the spectrum. The parent sample also showed the presence of sulfur, but there was no evidence of a cover, and the sulfur and oxygen mappings showed similar dimensions as that of Te. The intensities of sulfur and oxygen peaks in the spectra were also lesser in the parent Te_1 sample, compared to the present case (see the Supporting Information, Figure S3). So the difference in thickness exhibited in this case is clearly due to the additional shell formed over the Te NWs, which elemental maps showed to contain a larger fraction of sulfur and oxygen.

We examined the samples using Raman spectroscopy. Te NWs are known to show fluorescence.[24a,30] As a result, the Raman spectra collected showed a huge fluorescence background. But in the lower wavenumber region, we were able to identify some new features in the samples containing thiols. Figure 6A shows a spectrum taken from pristine Te NW and Te NW containing 2 mM DMSA. The second spectrum was taken after 24 h of incubation of the sample. A clear peak around 500 cm^{-1} can be seen in the DMSA containing sample which is absent in the pristine NW. This feature is absent in parent DMSA also. Enlarged view of the lower wavenumber region of the spectrum is given in the inset. Disulfides are known to show a Raman feature around 450−520 cm^{-1} region.[31b,32] This points to the presence of disulfide bonds in the sample, formed by the oxidation of thiols.[33] The fluorescence exhibited by Te NW was used for imaging the bundle of NWs. Figure 6B shows the fluorescence image of a bundle of NW taken with a Raman instrument.

(32) (a) Minouraa, Y.; Oriyo, T. *J. Chem. Soc.* **1951**, 1332. (b) Nakayama, H.; Hirami, S.; Tsuhako, M. *Chem. Lett.* **2004**, *33*, 712. (c) Van Wart, H. E.; Lewis, A.; Scheraga, H. A.; Saeva, F. D. *Proc. Natl. Acad. Sci. U.S.A.* **1973**, *70*, 2619. (d) Murty, K. V. G. K.; Venkataramanan, M.; Pradeep, T. *Langmuir* **1998**, *14*, 5446. (e) Venkataramanan, M.; Skanth, G.; Bandyopadhyay, K.; Vijayamohanan, K.; Pradeep, T. *J. Colloid Interface Sci.* **1999**, *212*, 553.
(33) (a) Klimmek, R.; Krettek, C.; Werner, H. W. *Arch. Toxicol.* **1993**, *67*, 428. (b) Andersen, O. *Chem. Rev.* **1999**, *99*, 2683. (c) Maiorino, R. M.; Xu, Z. F.; Aposhian, H. V. *J. Parmacol. Exp. Ther.* **1996**, *277*, 375.

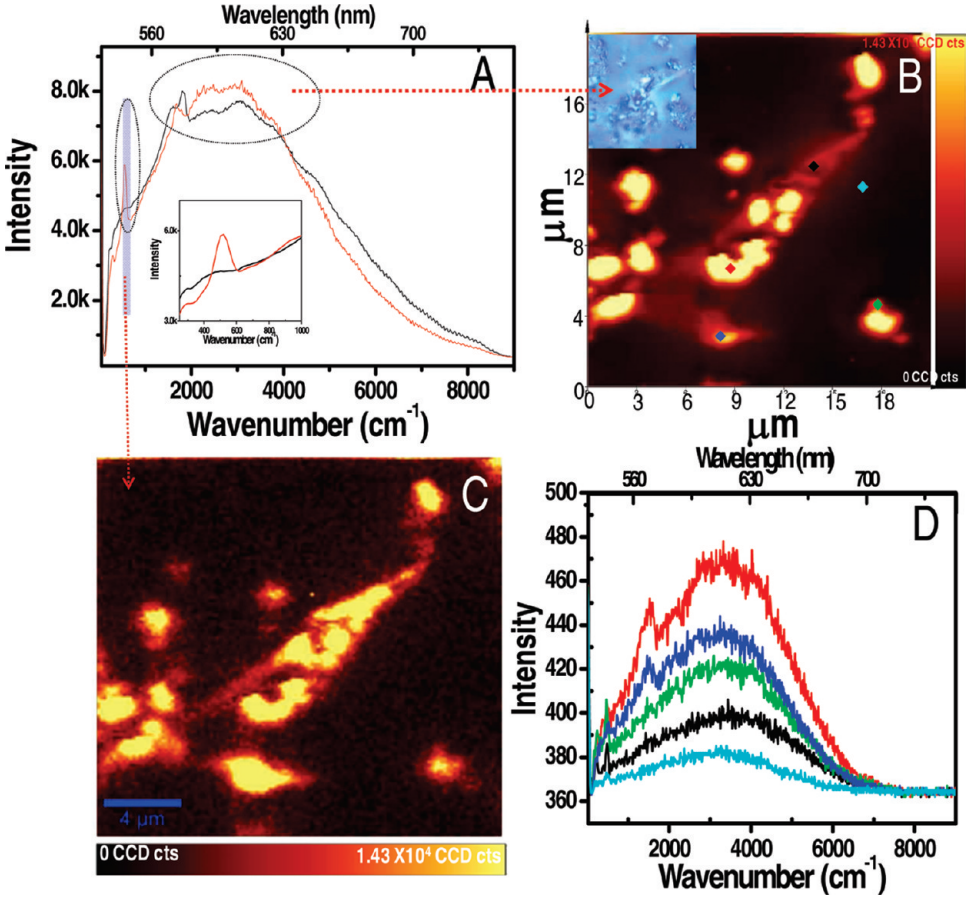

Figure 6. (A) Raman spectra taken from pristine Te NW (black trace) and DMSA-containing sample (2 mM, red trace) showing the presence of disulfide in the latter. Inset shows the enlarged view of the lower wavenumber region showing the disulfide peak clearly. (B) Fluorescence image taken from the Te NW-DMSA sample using fluorescence of Te NW in the 532−800 nm region. Inset shows the optical image of the same region under white light illumination. (C) Raman spectral image generated from the Raman frequency range of 380−510 cm^{-1}, corresponding to disulfide, showing the disulfide distribution in the sample. (D) Reconstructed image spectra from the spots marked in Figure 6B. The spherical structures seen in the images are bundles of Te NWs and not spherical particles. The upper scale in A and D correspond to the fluorescence.

With the resolution of the microscope, it was practically impossible to observe single Te NWs. So only bundles were seen. It has to be noted that the spherical structures seen in the image are not spherical nanoparticles but bundles of Te NW. Inset shows the corresponding optical image under white light illumination. Figure 6C shows a Raman spectral image generated from the region between 380 and 510 cm^{-1}, which corresponds to disulfides. The image showed close similarity to the fluorescence image generated from the full spectrum implying that the structure contains disulfide also. All these observations point to the fact that the shell formed in the reaction may be composed of disulfide. Anisotropic nanostructures are known to enhance Raman intensities. We observed that the Raman intensities obtained from different regions of the image are different. Figure 6D shows the image spectrum reconstructed from different regions of the fluorescence image. We can see that the intensity is maximum from the region where bundles of NWs are present. Both the fluorescence from the NW and the Raman feature from the disulfide formed due to the reaction have maximum intensity where the nanowire bundles are present (red trace). The lowest intensity was obtained from the region near to substrate where NWs are not present (cyan trace). This emphasizes the point that the distribution of Te NW and disulfide species occur in the same region. This also supports the proposition that the thiols are getting converted to disulfides, as proposed.

TEM showed that as the concentration of thiol increased, the shell thickness also increased. Samples having different concentrations of thiols were analyzed using Raman spectroscopy. In the full range, all these samples showed fluorescence. But in the lower wavenumber region, some interesting characteristics were visible. Therefore, this area was examined carefully. Figure 7A shows the Raman spectra taken in the lower wavenumber region from samples containing different conc. of DMSA. All spectra were taken after 12 h of incubation. Parent Te NW showed mainly two features, one centered at 148 cm^{-1} presumably because of the presence of tellurium oxide present on Te NW.[34] An additional peak was seen around 270 cm^{-1}. Te(0) is reported to show a feature at 270 cm^{-1} due to the second order E mode. Therefore, in the case of the parent Te NW sample, Te(0) in the bulk may be covered with a small amount of Te oxides on the surface as reported earlier.[34] In sulfur containing Te samples, it is reported that the Te−S bond can show a

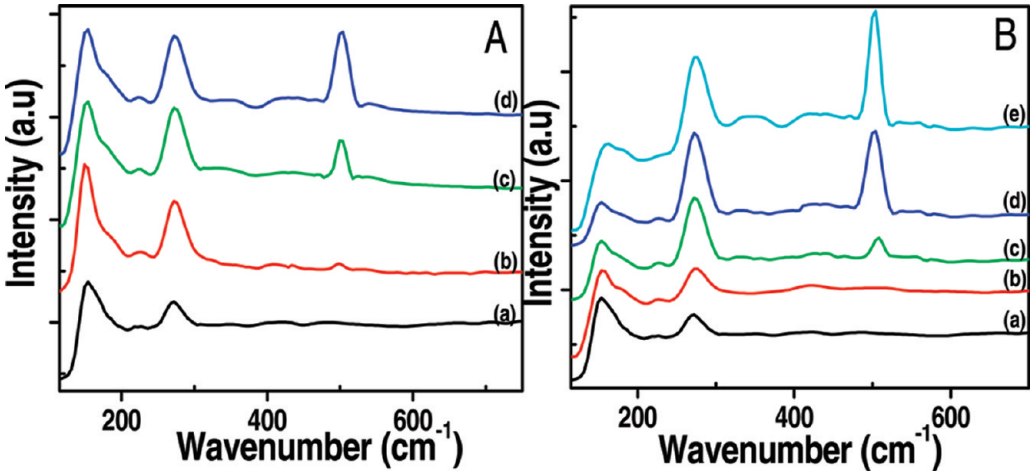

Figure 7. Raman of the Te NW samples. (A) In the presence of different concentrations of DMSA: (a) pristine Te NW, (b) 0.5, (c) 2, and (d) 5 mM DMSA, respectively. (B) Sample containing 2 mM DMSA analyzed at different times: (a) pristine Te NW, (b) 0, (c) 6, (d) 12, and (e) 24 h, respectively.

feature around the same region.[34d] In the as prepared Te NW sample the surfactant SDS has a sulfate group and so this probability is also there and the feature at 270 cm^{-1} may be a combination of both of these, although Te−S bonding due to sulfate is unlikely.

A third feature around 500 cm^{-1} began to appear as the thiol was added into the solution. The intensity of this peak increased as the concentration of DMSA increased. Disulfides are known to show a peak in the region 450−520 cm^{-1}.[32] We attribute this peak to disulfides because thiols are known to form disulfides.[33] The EDS analysis showed sulfur content in the shell. From the Raman spectroscopic data, it can be concluded that the sulfur is mostly in the disulfide form. We found that the disulfide feature increases in intensity as the concentration of DMSA added is increased. This confirms that the thiols added into the Te NW are mostly getting converted into disulfide. The change in the form of thiol species in the Te NW was followed time dependently. Figure 7B shows the time-dependent Raman study of Te NW sample containing 2 mM DMSA. Parent Te NW as well as sample immediately after addition of DMSA (0 h) showed only two peaks, as discussed earlier. But in the spectra after 6 h of reaction, the disulfide peak begins to appear and the peak due to tellurium oxide decreases in intensity. This trend was continued as time progressed. After 12 h of addition, there was a prominent signature of disulfide and the Te−O signature decreased in intensity further. The feature at 270 cm^{-1} was becoming more and more prominent in concordance with the increase in intensity of disulfide peak as well as the decrease in intensity of the Te−O feature. This suggested the possibility of a redox-like reaction between thiols and tellurium oxide, resulting in the oxidation of thiols to disulfide while tellurium oxide is reduced to Te(0). All the spectral features are in accordance with the data obtained from EDS mapping, suggesting that this redox reaction may be the reason for the formation of the core−shell structure.

This was again verified using XPS. Pristine Te NW showed a small extent of oxidation in XPS. Figure 8A shows the XPS spectrum of the Te 3d region of the parent Te NW and the Te NW-DMSA sample (a and b, respectively). In addition to the Te(0) 3d peaks, we can see signatures of oxidized Te in trace a. This confirmed the presence of tellurium oxides in the NW sample, which is consistent with an earlier report.[30] The sample containing 2 mM DMSA after incubating for 24 h, was also analyzed using XPS. Plot b in Figure 8A shows the XPS in the Te 3d region of the above sample. We can clearly see that the all the oxidized peaks have been reduced and only Te(0) is shown in the spectrum confirming the reduction of tellurium oxide to Te(0) as proposed earlier. Sulfur region was also scanned (Figure 8B). Pristine Te NW showed a single S 2p peak (Figure 8Ba) corresponding to sulfur with an oxidation state of six corresponding to sulfate, mostly from SDS, proving that it is indeed present on Te NWs.[35] Te NW-DMSA sample (Figure 8Bb) showed, in addition to sulfate, another feature due to the lower oxidation state as well. This is presumably due to the thiols or disulfides present in the sample. Three main features at 163.3, 164.5, and 168.8 eV were observed. Free thiol or thiolates are reported to have S 2p signal in the range of 161−162.5 eV.[35a,36] For disulfides, the S 2p comes in the range of 163−165 eV.[32e,37] We got the XPS features at 163.3 and 164.5 eV for S $2p_{3/2}$ and $2p_{1/2}$,

(34) (a) Qin, A.; Fang, Y.; Tao, P.; Zhang, J.; Su, C. *Inorg. Chem.* **2007**, *46*, 7403. (b) Baesman, S. M.; Bullen, T. D.; Dewald, J.; Zhang, D.; Curran, S.; Islam, F. S.; Beveridge, T. J.; Oremland, R. S. *Appl. Environ. Microbiol.* **2007**, *73*, 2135. (c) Frost, R. L. *Spectrochim. Acta, A* **2009**, *72*, 903. (d) Alía, J. M.; Edwards, H. G. M.; García-Navarro, F. J. *J. Mol. Struct.* **1999**, *508*, 51. (e) Song, J.-M.; Lin, Y.-Z.; Zhan, Y.-J.; Tian, Y.-C.; Liu, G.; Yu, S.-H. *Cryst. Growth Des.* **2008**, *8*, 1902.

(35) (a) Moulder, J. F.; Stickle, W. F.; Soble, P. E.; Bomben, K. D. *Handbook of X-ray Photoelectron Spectroscopy*; Perkin-Elmer Corporation: Eden Prairie, MN, 1992. (b) Mekhalif, Z.; Riga, J.; Pireaux, J.-J.; Delhalle, J. *Langmuir* **1997**, *13*, 2285. (c) Etahiri, A.; Humbert, B.; El Kacemi, K.; Marouf, B.; Bessière, J. *Int. J. Miner. Process.* **1997**, *52*, 49.

(36) (a) De Nadaï, C.; Whelan, C. M.; Perollier, C.; Clarkson, G.; Leigh, D. A.; Caudano, R.; Rudolf, P. *Surf. Sci.* **2000**, *454*, 112. (b) Kang, S. Y.; Kim, K. *Langmuir* **1998**, *14*, 226.

(37) (a) Castner, D. G.; Hinds, K.; Grainger, D. W. *Langmuir* **1996**, *12*, 5083. (b) Porter, L. A.; Ji, D.; Westcott, S. L.; Graupe, M.; Czernuszewicz, R. S.; Halas, N. J.; Lee, T. R. *Langmuir* **1998**, *14*, 7378. (c) Chen, T.-Y.; Chen, S.-F.; Sheu, H.-S.; Yeh, C.-S. *J. Phys. Chem. B* **2002**, *106*, 9717.

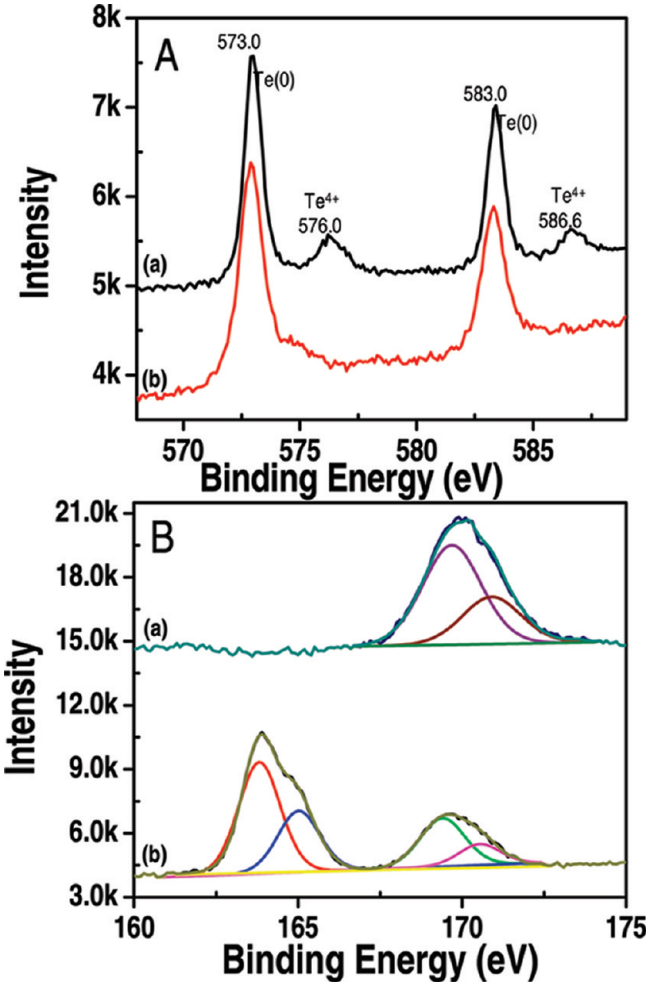

Figure 8. XPS spectra of (A) Te 3d and (B) S 2p regions of (a) pristine Te NW and (b) Te NW-DMSA sample (2 mM), after incubating for 24 h.

respectively, emphasizing that the thiols added into the Te NW were converted to disulfides.

The oxidation of thols to disulfides is a well-known process.[32,37] Raman spectra showed that as the disulfides are getting formed, the tellurium oxides are getting reduced into elemental tellurium. This was again proved by XPS. All these point to a redox-like reaction between tellurium oxide and thiols through which the latter is getting oxidized to disulfides and the former is getting reduced to Te(0). The redox potential of TeO_2/thiol couple also is favorable for such a reaction. Reduction potential of TeO_2/Te is 0.568 V.[23b] The reduction potential of disulfide/thiol couple for thioacids is around −1.36 V.[38] Hence a redox reaction between TeO_2 and DMSA, which has two thiol groups, is probable. Because in the reaction mixture, a third component in the form SDS is present, it may be getting involved in the process and our proposal is that, by a combination of this surfactant and the formed disulfide, a thick shell is getting formed over the Te NW. XPS showed the presence of both SDS and disulfide in the sample emphasizing the point.

(38) (a) Surdhar, P. S.; Armstrong, D. A. *J. Phys. Chem.* **1987**, *91*, 6532. (b) Surdhar, P.; Armstrong, D. A. *J. Phys. Chem.* **1986**, *90*, 5915.

Because the surfactant SDS plays an important role in the shell formation, the reaction was also carried out in the reduced concentration of SDS. The NW solution was repeatedly centrifuged and redispersed in distilled water to remove the excess SDS as much as possible. Te_2 did not show any change in UV/vis spectra even after 4 rounds of centrifugation and redisperision cycles (see the Supporting Information, Figure S4). The Peak I and Peak II remained unchanged. The intensity was almost double of Te_1. This is expected since the volume of the sample was reduced to half its initial volume and corresponding increase was seen in the intensity of the absorption spectra. Other than this, no visible changes were observed. The sample was stable and remained as a stable suspension, without any aggregation. The peak positions also remained unchanged. To Te_2 sample, as discussed in the Experimental Section, 2 mM DMSA was added. We found that the NWs tend to bend. Figure 9 shows the TEM images of the bent NW after the addition of DMSA. The large area image shows a number of bent NWs. The inset shows a single NW with multiple bends along the length of the NW. We can clearly see that a thin shell is still present on the surface of the NW, which is clearly seen in the inset of Figure 9A. Figure 9B shows the lattice-resolved image of such a bend in the NW. The interesting observation is that around the bend region, the lattice structure of the NW has been modified. Mostly, defects are being created on the {001} surface of the NW. The area marked by a rectangle in Figure 9B shows this aspect clearly. We can also see some protrusion on the surface. Parent NWs were single-crystalline and the surface was clean without any depressions or protrusions (see the Supporting Information, Figures S7 and S9). But after the reaction, the bent NWs had several protrusions all through the wire body (inset of Figure 9A). HRTEM image in Figure 9B also shows the small protrusions (dotted circles) around the bend region, which may be the newly added atoms during the reaction.

HRTEM of parent NW, Te_2 (see the Supporting Information, Figures S7 and S9) showed that the surface of Te NW is mainly composed of {001}, {010}, and {110} facets. Before the reaction, the NW were perfectly single-crystalline without any defects or dislocations. We found that after the reaction, the lattice structure of the Te NW gets distorted. Many defects and stacking faults were seen all through the NW after the reaction. In most of the NWs investigated, the {111} and {001} facets were prominent after the reaction. Most of these defects were seen on the {001} facet, which can be clearly seen in Figure 9B. In the area marked in a rectangle, we can see that there is a lattice mismatch near the place where the NW bends. There is also a clear disappearance of lattice in certain region. This may be due to the defects and reconstructions induced by the reaction. All these point to a large-scale lattice distortion of Te NW during the reaction.

The samples were analyzed using EDAX (Figure 10) to identify the elemental characteristics of the sample and to understand the difference between the present case (Te_2)

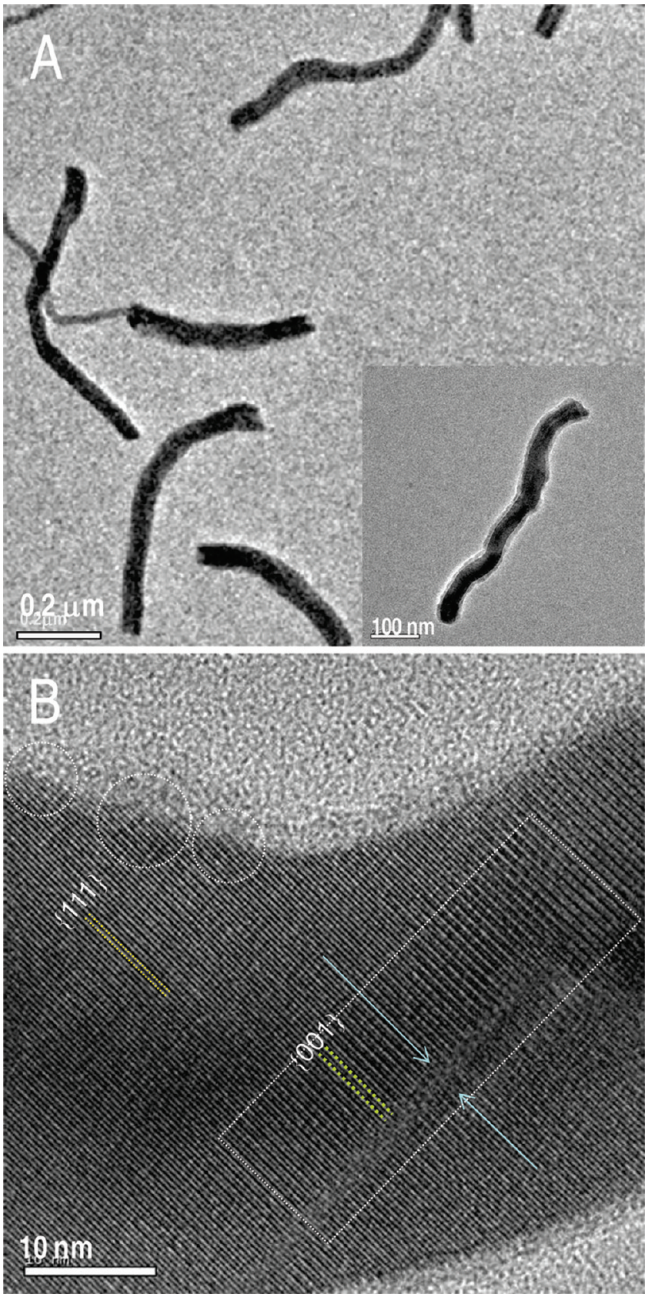

Figure 9. (A) Large-area TEM image of bent NW after reaction with DMSA at reduced surfactant concentration. (B) Lattice-resolved image of the bend of a NW where the area with defects and possible reconstructions is marked with a rectangle. Disappearance of lattice planes in-between the arrows can be seen. The idealized NW surface without defects is now modified. There are projections indicating added atoms marked by circles.

and the case in which excess surfactant was present (Te_1). We found that in the bent NWs, the amount of sulfur present has reduced considerably. In the spectrum, we can see that the sulfur peak intensity has reduced, compared to Te_1 (see the Supporting Information Figure S3). This is understandable because most of the SDS has been removed by centrifugation; because much less surfactant is present, the shell formation on NW is not possible. The disulfide formed during the reaction, getting attached to the NWs may be very small because the amount of SDS is minimal. There was a slight increase in the sulfur intensity in the spectrum when compared to the parent Te_2 (see the

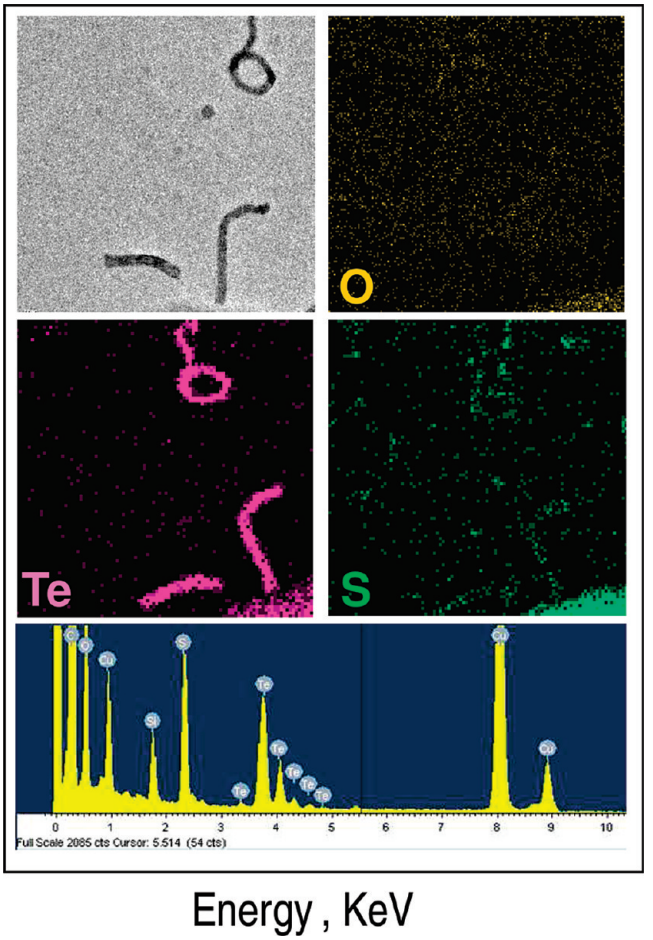

Figure 10. EDAX spectrum and elemental mapping of the Te_2 sample containing 2 mM DMSA showing the bent NW.

Supporting Information, Figure S5), emphasizing that there is still reaction with thiol and a thin shell is formed. But because the concentration of the surfactant present is not large enough, a thick shell is not formed, resulting in bending.

Nanowires that were defect-free before the reaction were found to be completely changed after the reaction. The NW sample was quite monodisperse before the reaction. But after the reaction, the sample lost its monodispersity. This could be because the kinetics of the reaction throughout the NW body, is not the same. This is because of the nonuniform oxide cover and the inhomogeneities in the surfactant cover. The length and diameter is changing because of the reaction with DMSA. Figure 9A shows an HRTEM image showing bent NWs having different length and diameter. Most of the NWs after reaction showed defects extending all through the NW body. In some cases, a complete raw of atoms was missing. Figure S6 in the Supporting Information shows a HRTEM image of such a single Te NW with defects. Figure S6B shows the lattice-resolved image of the region marked by yellow rectangle in Figure S6A. A complete raw of atoms was found to be missing, indicated by the arrow in the figure. We can see that similar defects are present in several places, wherever the NW is bent. Figure S6C in the Supporting Information shows the lattice-resolved image

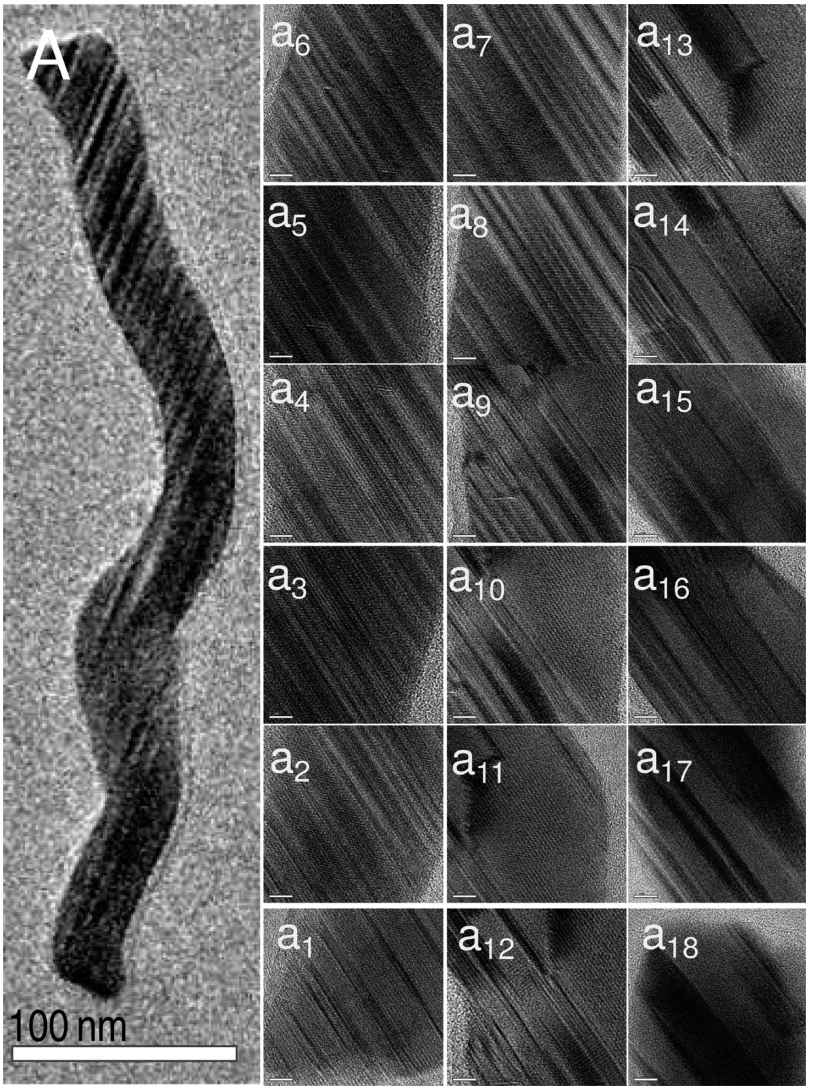

Figure 11. (A) HRTEM image of a single bent NW. (a_1-a_{18}) Lattice-resolved TEM images taken along the length of the bent NW, starting from the tip, showing the defects round the bend. Scale bar in each image 5 nm. The lattice-resolved images are rotated 90° in comparison to the large-area image.

of the region marked by green rectangle in Figure S6A, again showing a large number of defects in the crystal.

To compare the lattice structure of parent NW and the bent NW and to study the defect formation during the reaction, we extensively analyzed these structures using HRTEM. Parent NWs were perfectly single-crystalline as shown in Figure 1D. The surface structure of the parent NWs was comprehensively analyzed (see the Supporting Information, Figure S7). Figure S7a_1-a_{14} shows the consecutive lattice-resolved images taken from one end of the NW to the other, along its length. We found that the NW is single-crystalline, devoid of defects. The surface was mainly found to be composed of {001}, {010}, and {110} planes as reported earlier.[24a,33] The lattice structure was found to be similar all through the NW; no disruption of lattice symmetry was seen, and the structure was found to be well-preserved without even minor defects. The fast Fourier transforms (FFTs) generated from them (a_1-a_{14}) also confirmed the single-crystalline nature (see the Supporting Information, Figure S7b_1-b_{14}). Figure 11 shows the HRTEM study of a bent NW. In it (Figure 11a_1-a_{18}), several defects are present on the NW body because of bending. Defects were especially prominent around the area where the NW is bent. This was again confirmed by consecutive FFTs generated form the lattice-resolved images a_1-a_{18} (see the Supporting Information, Figure S8).

Most of the bent NWs had a large number of defects on the wire body. But in some cases, the single-crystalline nature of the NW itself was found to be lost at the regions where they bend and it showed a polycrystalline character because of the reaction. Selected area electron diffraction (SAED) pattern and FFTs derived from this region clearly showed this change in crystallinity (Figure 12). Figure 12A shows a single bent NW. We can see that still there is a thin shell surrounding the NW. Figure 12B shows the lattice-resolved TEM image taken from the portion marked in Figure 12A. We can see that the area is polycrystalline and has a large number of defects. The Inverse FFT (IFFT) generated from the same area (Figure 12C) again points to the polycrystalline nature. The inset in Figure 12A shows the FFT (a) and SAED (b)

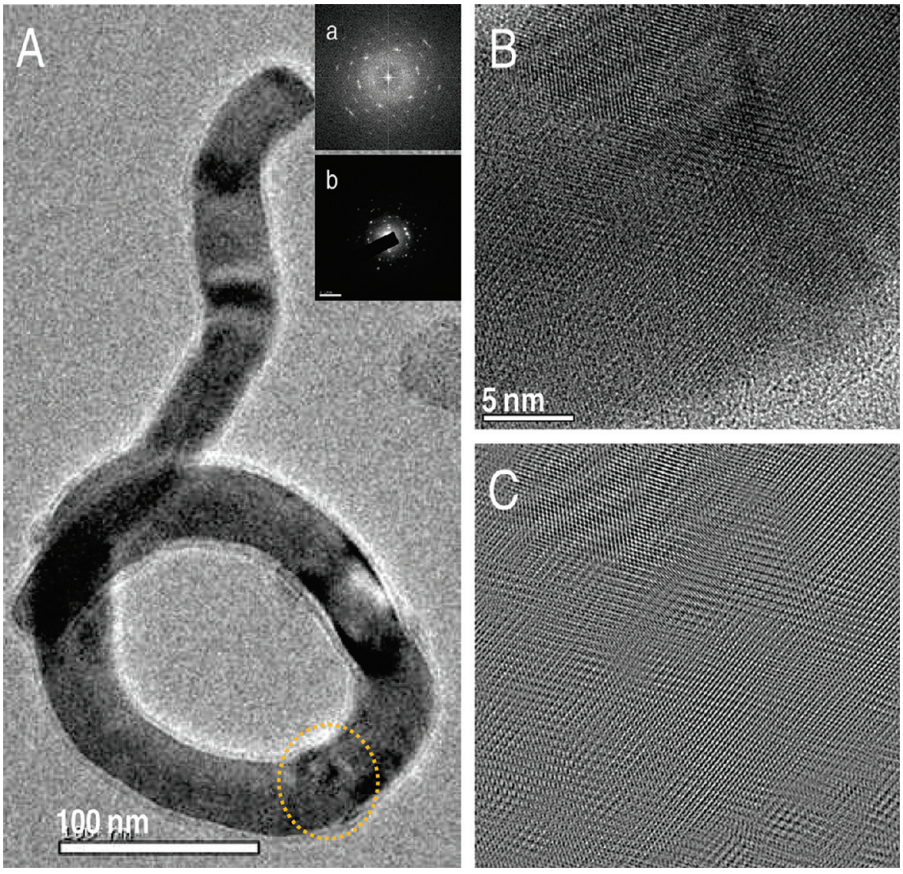

Figure 12. (A) TEM micrograph of a single bent NW. (B) Lattice-resolved image and (C) IFFT image from the portion marked in A of bent Te NW showing the change to polycrystalline nature. Insets a and b are FFT and SAED patterns from the same area emphasizing the polycrystalline nature.

patterns obtained from the same area. It is clear that the single-crystalline nature of the sample has been lost.

We think that because of the strain created by the reaction and addition of more number of Te atoms into the parent structure, the geometry of the NW undergoes distortion. To accommodate the extra Te atoms, we believe that primarily the {001} plane of the NW undergoes buckling and rises above the layer. This may be the reason for the sudden disappearance of lattice in some region since because of this buckling, the lattice plane goes away from the focal plane and gets smeared. Figure 9B showed such a case clearly. Around the bent region, we can see a sudden disappearance of lattice and above and below that, the {001} lattice planes are seen very clearly, supporting our proposition. The buckling of the lattice and the unavailability of excess surfactant to stabilize the resultant structure is believed to be the reason for the bending of NWs.

Te is known to be resistant to oxidation at normal temperatures and pressures.[39] The reaction between Te and oxygen or air is reported to happen only at temperatures on the order of 60 °C. XPS data of the samples (as-prepared TeNW, Te_1, and Te_2) in the Te 3d region are compared in the Supporting Information, Figure S10. Although no oxide was seen in the as prepared sample, it appears in Te_1 and the intensity is much larger in Te_2. Thus slow reaction at the unprotected surfaces may be the reason for the development of an oxide layer on the Te NW samples after centrifugation. This oxide layer is thinner than 2.8 nm, the mean free path of Te 3d electrons of 1486.6 eV kinetic energy[40] as the underlying Te(0) is seen in XPS. However, the TEM images of Te_1 (Figure 1) and Te_2 (see the Supporting Information, Figure S7) show no distinct change in the lattice structure. An oxide layer of ~3 nm thickness would have been seen in HRTEM. Thus we believe that the layer is very thin, on the order of 1 nm. We note that even for thin films of 200 nm thickness, the oxide layer formed on treatment at high temperatures and 800 Torr pressure was thin, ranging from 0.9 nm to 2 nm.[39]

During repeated centrifugation, the protecting layer of SDS is also disrupted. At these locations, greater oxidation can occur with time. Oxygen required for the reaction is available in the solution. The layer may not be uniform as well and the localized concentration of TeO_2 may be quite large in some places in Te_2; this region might give rise to bends. TeO_2 concentrations on different NWs in Te_2 can be different, which may result in the different extent of bending in various nanowires.

The energetics of the reaction is not well understood at this time. The bending of NWs is normally achieved by the application of high stress or energy.[40] But in the present case, at room temperature, without any external

(39) (a) Dutton, W. A.; Cooper, W. C. *Chem. Rev.* **1966**, *66*, 657. (b) Musket, R. G *Surf. Sci.* **1978**, *74*, 423.

(40) Powel, C. J.; Jablonski, A. *J. Phys. Chem. Ref. Data* **1999**, *28*, 19.

aid, the NWs bend. So the energy needed for bending the structure should be produced during the reaction in the medium. It is known that surface defects can get formed because of reactions.[41] Here the principal reactions happening in the medium are the reduction of TeO_2 to Te(0) and the oxidation of thiols to disulfides. But the reduction reactions are normally endothermic and oxidation reactions are exothermic. Because the reaction is redox in nature and is spontaneous and also proceeds without any external aid like heat, irradiation, etc., the total reaction should be exothermic. A part of this excess energy is believed to be utilized for the deformation.

Summary and Conclusions

Te NW reactivity with thiols has been probed taking DMSA as a model molecule. It was found that depending upon the presence and absence of surfactant, the reaction product differed drastically. When excess surfactant was present, a shell was formed around the NW giving it a "core−shell-like" structure. Samples were analyzed using various spectroscopic and microscopic techniques. UV/vis showed that peak I of Te NW get smeared as the concentration of DMSA increases. TEM images showed that as the concentration of DMSA increases, the shell thickness also increases. Through Raman spectroscopy and XPS, it was proposed that there is a redox-like reaction between the thiol and TeO_2 present on the NW surface, which results in the reduction of TeO_2 to Te(0) and the oxidation of thiol to disulfide. This is considered as the cause of the structural changes in the NW. EDAX showed a considerable reduction in sulfur in Te_2 compared to Te_1. In Te_2, because of the limited amount of surfactant, the capping is not efficient. This leads to reconstructions and finally bending of NW. In Te_1, because excess surfactant is present, the NWs can be well-protected and the structure can be preserved. Therefore, a shell is formed that keeps the structure of the NW intact. Shells formed using biofriendly molecules such as cysteine, glutathione, or proteins may make Te NWs more biofriendly for various biological applications. The thick shells may reduce the reactivity of the nanowires with external agents.

Acknowledgment. We thank the Nanoscience and Nano Mission of Department of Science and Technology (DST), Government of India, for supporting our research program.

Supporting Information Available: UV/vis spectral changes accompanied by the addition of cystien, butanol, isopropyl amine, and salicylic acid; comparison of UV/vis spectra of free thiol and Te_1 sample containing thiol, EDAX analysis of pristine NW samples, Te_1, and Te_2; UV/vis spectra of as-prepared Te NW, Te_1 and Te_2, FFTs and inverse FFTs of parent NWs, and bent NWs; XPS spectra of as-prepared Te NW, Te_1, and Te_2; additional HRTEM images of bent NWs (PDF). This material is available free of charge via the Internet at http://pubs.acs.org.

(41) (a) Weber, F.; Schestakow, I.; Roters, F.; Raabe, D. *Adv. Eng. Mater*. **2008**, *10*, 737. (b) Li, L.; Yang, Y.; Huang, X.; Li, G.; Zhang, L. *J. Phys. Chem. B* **2005**, *109*, 12394. (c) Makeev, M. A.; Srivastava, D.; menon, M. *Phys. Rev. B* **2006**, *74*, 165303. (d) McDowell, T. M.; Leach, A. M.; Gall, K. *Modell. Simul. Mater. Sci. Eng*. **2008**, *16*, 045003.

(42) (a) Ye, J. H.; Pe′rez-Murano, F.; Barniol, N.; Abadal, G.; Aymerich, X. *J. Vac. Sci. Technol., B* **1995**, *13*, 1423. (b) Yoshimura, M.; Ono, I.; Ueda, K. *Appl. Surf. Sci*. **1998**, *130*, 276. (c) Wu, C. I.; Kahn, A.; Wickenden, A. E.; Koleske, D.; Henry, R. L. *J. Appl. Phys*. **2001**, *89*, 425. (d) Umezu, I.; Sugimura, A.; Makino, T.; Inada, M.; Matsumoto, K. *J. Appl. Phys*. **2008**, *103*, 024305.